Inorg. Chem. **2004**, *43*, 3812–3824

Supramolecular Mn(II) and Mn(II)/Mn(III) Grid Complexes with $[Mn_9(\mu_2\text{-}O)_{12}]$ Core Structures. Structural, Magnetic, and Redox Properties and Surface Studies

Liang Zhao,[†] Zhiqiang Xu,[†] Hilde Grove,[†] Victoria A. Milway,[†] Louise N. Dawe,[†] Tareque S. M. Abedin,[†] Laurence K. Thompson,*[,†] Timothy L. Kelly,[†] Rosemary G. Harvey,[†] David O. Miller,[†] Laura Weeks,[‡] Joseph G. Shapter,[‡] and Kenneth J. Pope[‡]

Department of Chemistry, Memorial University, St. John's, Newfoundland A1B 3X7, Canada, and School of Chemistry, Physics and Earth Sciences, Flinders University of South Australia, Bedford Park, South Australia 5042, Australia

Received November 14, 2003

A series of [3 × 3] $Mn(II)_9$, antiferromagnetically coupled, alkoxide-bridged, square grid complexes, derived from a group of "tritopic" dihydrazide ligands, is described. The outer ring of eight Mn(II) centers in the grids is isolated magnetically from the central Mn(II) ion, leading to an $S = 0$ ground state for the ring, and an $S = 5/2$ ground state overall in each case. Exchange in the $Mn(II)_8$ ring can be represented by a 1D chain exchange model. Rich electrochemistry displayed by these systems has led to the production of Mn(II)/Mn(III) mixed-oxidation-state grids by both electrochemical and chemical means. Structures are reported for $[Mn_9(2poap)_6](C_2N_3)_6\cdot 10H_2O$ (**1**), $[Mn_9(2poap)_6]_2[Mn(NCS)_4(H_2O)]_2(NCS)_8\cdot 10H_2O$ (**2**), $[Mn_9(2poapz)_6](NO_3)_6\cdot 14.5H_2O$ (**3**), $[Mn_9(2popp)_6](NO_3)_6\cdot 12H_2O$ (**4**), $[Mn_9(2pomp)_6](MnCl_4)_2Cl_2\cdot 2CH_3OH\cdot 7H_2O$ (**5**), and $[Mn_9(Cl2poap)_6](ClO_4)_9\cdot 7H_2O$ (**6**). Compound **1** crystallized in the tetragonal system, space group $P4_2/n$, with $a = 21.568(1)$ Å, $c = 16.275(1)$ Å, and $Z = 2$. Compound **2** crystallized in the triclinic system, space group $P\bar{1}$, with $a = 25.043(1)$ Å, $b = 27.413(1)$ Å, $c = 27.538(2)$ Å, $\alpha = 91.586(2)°$, $\beta = 113.9200(9)°$, $\gamma = 111.9470(8)°$, and $Z = 2$. Compound **3** crystallized in the triclinic system, space group $P\bar{1}$, with $a = 18.1578(12)$ Å, $b = 18.2887(12)$ Å, $c = 26.764(2)$ Å, $\alpha = 105.7880(12)°$, $\beta = 101.547(2)°$, $\gamma = 91.1250(11)°$, and $Z = 2$. Compound **4** crystallized in the tetragonal system, space group $P4_12_12$, with $a = 20.279(1)$ Å, $c = 54.873(6)$ Å, and $Z = 4$. Compound **5** crystallized in the tetragonal system, space group $I\bar{4}$, with $a = 18.2700(2)$ Å, $c = 26.753(2)$ Å, and $Z = 2$. Compound **6** crystallized in the triclinic system, space group $P\bar{1}$, with $a = 19.044(2)$ Å, $b = 19.457(2)$ Å, $c = 23.978(3)$ Å, $\alpha = 84.518(3)°$, $\beta = 81.227(3)°$, $\gamma = 60.954(2)°$, and $Z = 2$. Preliminary surface studies on Au(111), with a Mn(II) grid complex derived from a sulfur-derivatized ligand, indicate monolayer coverage via gold–sulfur interactions, and the potential for information storage at high-density levels.

Introduction

Tritopic ligands with a 2,6-pyridine dihydrazone core react with transition-metal salts (e.g., Mn(II), Fe(II), Fe(III), Co(II), Ni(II), and Cu(II)) in a high-yield self-assembly process to form nonanuclear, alkoxide-bridged [3 × 3] grid complexes as a major class (Chart 1).[1−8] Other coordination modes with ligands of this type involve the formation of self-assembled octanuclear alkoxide-bridged "pinwheel" grid-

* Author to whom correspondence should be addressed. Fax: (709) 737-3702. E-mail: lthomp@mun.ca.
[†] Memorial University.
[‡] Flinders University of South Australia.

(1) Zhao, L.; Matthews, C. J.; Thompson, L. K.; Heath, S. L. *J. Chem. Soc., Chem. Commun.* **2000**, 265.
(2) Zhao, L.; Xu, Z.; Thompson, L. K.; Heath, S. L.; Miller, D. O.; Ohba, M. *Angew. Chem., Int. Ed.* **2000**, *39*, 3114.
(3) Waldmann, O.; Koch, R.; Schromm, S.; Müller, P.; Zhao, L.; Thompson, L. K. *Chem. Phys. Lett.* **2000**, *332*, 73.
(4) Waldmann, O.; Zhao, L.; Thompson, L. K. *Phys. Rev. Lett*. **2002**, *88*, 066401.
(5) Zhao, L.; Xu, Z.; Thompson, L. K.; Miller, D. O. *Polyhedron* **2001**, *20*, 1359.
(6) Thompson, L. K.; Zhao, L.; Xu, Z.; Miller, D. O.; Reiff, W. M. *Inorg. Chem*. **2003**, *42*, 128.
(7) Xu, Z.; Thompson, L. K.; Miller, D. O. *Polyhedron* **2002**, *21*, 1715.
(8) Thompson, L. K. *Coord. Chem. Rev*. **2002**, *233*−*234*, 193.

10.1021/ic030319v CCC: $27.50
Published on Web 05/29/2004

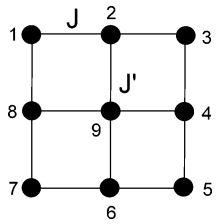

Figure 1. Magnetic exchange model in M_9 grids.

Chart 1

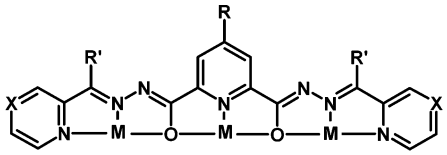

(X=CH) 2poap (R=H,R'=NH_2), 2popp (R=H,R'=Ph), 2pomp (R=H, R'=Me), Cl2poap (R=Cl, R'=NH_2), S2poap (R=S^- NH_4^+); (X=N) 2poapz (R=H, R'=NH_2).

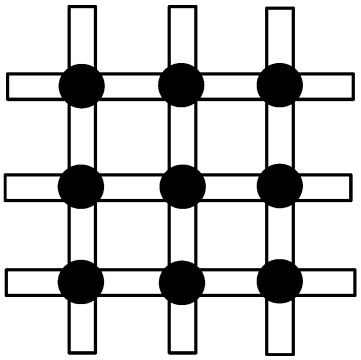

based clusters in the case of copper(II),[9,10] diazine (N_2)-bridged systems in a series of trinuclear copper(II) complexes,[11,12] and a novel Cu_{36} cluster involving an extended "pentatopic" dioxime ligand.[13] Intramolecular antiferromagnetic exchange prevails in the [3 × 3] grid complexes in most cases, except copper(II), where dominant intramolecular ferromagnetic exchange is observed in all examples. This also occurs in the octanuclear $Cu(II)_8$ complexes. The $Mn(II)_9$ complexes are a particularly interesting class, with $S = 5/2$ ground states, resulting from intramolecular antiferromagnetic exchange, and an exchange mechanism which is dominated by the eight Mn(II) atoms in the outer ring (Figure 1, $J \gg J'$). [3 × 3] "magnetic" grid complexes in this class are rare, and other nonmagnetic [3 × 3] examples are to our knowledge limited to a $Ag(I)_9$ pyridazine-bridged grid reported by Lehn.[14] Recent reports indicate that expanded, e.g., [4 × 4][15] and [4 × (2 × 2)][16] $Pb(II)_{16}$ grid architectures can be produced with bridging pyrimidine ligands.

The coordination compartments within the [3 × 3] grid structures formed by these tritopic ligands (Chart 1) are comprised of three different donor groupings: corner (*cis*-N_4O_2), side (*mer*-N_3O_3), and center (*trans*-N_2O_4) (vide infra). These differing coordination environments clearly lead to different properties at these metal ion sites, which is manifested in terms of, e.g., differing redox characteristics, and possibly differing spin ground-state situations, depending on the identity of the metal ion, and may even be useful for selective site occupancy in mixed-metal systems. The cobalt chemistry of grids with ligands in this class has shown that exposure to air can lead to mixed-oxidation-state Co(II)/Co(III) systems.[17] This is also possible for the $Mn(II)_9$ complexes, although reactions in air have not yet indicated any Mn(II) oxidation in general synthesis. Electrochemical studies however have shown clearly defined groups of redox waves in cyclic voltammetry, corresponding to oxidation of Mn(II) to Mn(III), within an easily accessible voltage range (0.5−1.5 V, vs SSCE), with a four-electron wave at $E_{1/2} =$ 0.61 V and four one-electron waves in the range $E_{1/2} = 0.92-$ 1.53 V for the complex $[Mn_9(2poap)_6](ClO_4)_6 \cdot 18H_2O$.[1] In the current paper we expand the scope of the $Mn(II)_9$ grid complexes within this class, examining new ligands, with various R and R′ groups (Chart 1), and the effect of these groups on structural, magnetic, and redox properties of the grid systems.

Functionalizing the ligands with S groups at the central 4-pyridine ring positions (e.g., Chart 1, R = S^-, SCH_2COOH, SCH_2Ph, etc.) has produced $Mn(II)_9$ grids with soft sites exposed on both surfaces of the grid. Such grid systems are being examined as potential substrates for attachment to "flat" gold surfaces, and initial experiments have shown the formation of monolayers, with clearly defined surface-bound molecules.[18] Complexes of this type are being explored in terms of their functional bistability, and multistability, and their ability to store information or act as molecular "switches".

Experimental Section

Physical Measurements. Infrared spectra were recorded as Nujol mulls using a Mattson Polaris FT-IR instrument. Mass spectra were obtained with VG Micromass 7070HS (EI) and HP1100MSD (LCMS) spectrometers. UV/vis spectra were obtained with a Varian/Cary 5E spectrometer. Microanalyses were carried out by Canadian Microanalytical Service, Delta, Canada. Variable-temperature magnetic data (2−300 K) were obtained using a Quantum Design MPMS5S SQUID magnetometer with field strengths in the range of 0.1−5.0 T. Samples were prepared in gelatin capsules or aluminum pans, and mounted inside straws for attachment to the sample transport rod. Background corrections for the sample holder assembly and diamagnetic components of the complexes were applied. Electrochemical studies were carried out with a BAS 100B electrochemistry system, with a Pt working electrode, Pt counter

(9) Xu, Z.; Thompson, L. K.; Miller, D. O. *J. Chem. Soc., Chem. Commun.* **2001**, 1170.
(10) Milway, V. A.; Niel, V.; Xu, Z.; Thompson, J. K.; Grove, H.; Miller, D. O.; Parsons, S. R. *Inorg. Chem.* **2004**, *43*, 1874.
(11) Zhao, L.; Thompson, L. K.; Miller, D. O.; Stirling, D. R. *J. Chem. Soc., Dalton Trans.* **2001**, 1706.
(12) Milway, V. A.; Zhao, L.; Abedin, T. S. M.; Thompson, L. K.; Xu, Z. *Polyhedron* **2003**, *22*, 1271.
(13) Abedin, T. S. M.; Thompson, L. K.; Miller, D. O.; Krupicka, E. *J. Chem. Soc., Chem. Commun.* **2003**, 708.
(14) Baxter, P. N. W.; Lehn, J.-M.; Fischer, J.; Youinou, M.-T. *Angew. Chem., Int. Ed. Engl.* **1994**, *33*, 2284.
(15) Barboiu, M.; Vaughan, G.; Graff, R.; Lehn, J.-M. *J. Am. Chem. Soc.* **2003**, *125*, 10257.
(16) Onions, S. T.; Franklin, A. M.; Horton, P. N.; Hursthouse, M. B.; Matthews, C. J. *J. Chem. Soc., Chem. Commun.* **2003**, 2864.
(17) Zhao, L.; Kelly, T. L.; Thompson, L. K. Unpublished results.
(18) Weeks, L.; Thompson, L. K.; Shapter, J. G.; Pope, K. J.; Xu, Z. *J. Microsc.* **2003**, *212*, 102.

electrode, and SSCE and Ag/AgCl reference electrodes. Differential pulse voltammetry was carried out at a 20 mV/s scan rate (50 mV pulse amplitude, 50 ms pulse width) in an oxidative sweep. Bulk electrolytic oxidation was carried out using a Pt mesh working electrode, a Pt mesh counter electrode, and a Ag/AgCl reference electrode, with a HP6215A power supply connected to a high-impedance voltmeter. STM images were acquired with a Digital Instrument Nanoscope IV controller in combination with an STM base. Electrochemically etched tungsten tips were used.

Syntheses of the Ligands and Complexes. The ligands 2poap, 2poapz, and Cl2poap were synthesized as reported previously.[5,6] S2poap was prepared by the same route, by reaction of the precursor dihydrazide with the imino ester of 2-picolinic acid.[5,6] The dihydrazide was prepared from the corresponding diethyl ester ammonium 2,6-dicarbethoxypyridine-4-thiolate[19] by reaction with hydrazine.

2popp. 2-Benzoylpyridine (10.0 g, 0.055 mol) was dissolved in methanol (250 mL). Pyridine 2,6-dihydrazide (5.00 g, 0.026 mol) was added and the mixture refluxed overnight. The white solid formed was collected by filtration, washed with methanol and ether, and air-dried (yield 12.3 g, 92%). Mp: 275−278 ° C. Mass spectrum (LCMS, chloroform) (*m*/*z*): 526.5 (M + H). IR (ν, cm^{-1}): 3294 (OH, NH), 1695, 1558 (CO, CN), 997 (pyr). Anal. Calcd for $C_{31}H_{23}N_7O_2$: C, 70.85; H, 4.41; N, 18.66. Found: C, 70.73; H, 4.46; N, 18.88. 2pomp was obtained in a similar manner by reacting pyridine 2,6-dihydrazide with 2-acetylpyridine in methanol (yield 99%). Mp: 313−315° C. Mass spectrum (*m*/*z*): 401 (M•$^+$), 386 (M − CH_3), 323 (M − C_5H_4N), 240, 224, 182, 134, 106, 78. IR (ν, cm^{-1}): 3350 (NH), 1704, 1695 (CO), 992 (py). NMR (DMSO-d_6, ppm) 2.1 (s), 2.6 (s, CH_3), 7−9 (m, aromatic ring), 11.0 (s), 11.5 (s, NH). Anal. Calcd for $C_{21}H_{19}N_7O_2$: C, 62.83; H, 4.77; N, 24.42. Found: C, 62.47; H, 4.77; N, 24.67.

$[Mn_9(2popp)_6](NO_3)_6\cdot 12H_2O$ (4). $Mn(NO_3)_2\cdot 6H_2O$ (0.17 g, 0.59 mmol) was dissolved in methanol (20 mL). 2popp (0.10 g, 0.19 mmol) was added along with chloroform (10 mL) and the mixture warmed. The ligand dissolved, forming a pale-orange-colored solution. Red crystals formed after two weeks (yield 35%), which were suitable for structural determination. Anal. Calcd for $(C_{31}H_{21}N_7O_2)_6Mn_9(NO_3)_6\cdot(H_2O)_{12}$: C, 52.89; H, 3.58; N, 15.90. Found: C, 52.89; H, 3.37; N, 15.71.

$[Mn_9(2pomp)_6](MnCl_4)_2Cl_2\cdot 2CH_3OH\cdot 7H_2O$ (5). 2pomp (0.20 g, 0.50 mmol) was added to a solution of $MnCl_2\cdot 6H_2O$ (0.40 g, 2.0 mmol) in methanol (10 mL) and the mixture stirred with warming. The ligand quickly dissolved to give a pale-colored solution, and the subsequent formation of a bright yellow precipitate. $Mn(CH_3COO)_3\cdot 3H_2O$ (0.2 g, 0.75 mmol) was added, resulting in a clear, deep red solution. Stirring and heating were continued for 1 h, and the solution was filtered and then allowed to evaporate slowly at room temperature. Deep red prismatic crystals suitable for structural analysis were formed after several weeks. The structural sample was kept under mother liquor prior to structural analysis, due to crystal instability on exposure to air (yield 35%). No evidence was found for incorporation of Mn(III) in the complex, and it is assumed that the $Mn(CH_3COO)_3\cdot 3H_2O$ simply acted as a source of weak base (acetate) in the reaction, facilitating proton loss from the ligands. Anal. Calcd for $(C_{21}H_{17}N_7O_2)_6Mn_9(MnCl_4)_2Cl_2(CH_3OH)_2\cdot(H_2O)_7$: C, 43.36; H, 3.52; N, 16.59. Found: C, 43.40; H, 2.99; N, 16.78.

The other complexes were prepared under conditions similar to those under which **4** was prepared using the appropriate ligand and Mn(II) salt in methanol or methanol/acetonitrile or acetonitrile/water mixtures (yields >60%). For **1** and **2** the ligand and $Mn(NO_3)_2\cdot 6H_2O$ were reacted in the normal way, and then solutions of $Na(N(CN)_2)$ and NH_4NCS were added, respectively. All structural samples were stored under mother liquor prior to structural analysis because of crystal instability resulting from solvent loss on exposure to air. Analytical data: $[Mn_9(2poap)_6](C_2N_3)_6\cdot 10H_2O$ (**1**). Anal. Calcd for $(C_{19}H_{15}N_9O_2)_6Mn_9(C_2N_3)_6\cdot(H_2O)_{10}$: C, 43.50; H, 3.19; N, 28.99. Found: C, 43.68; H, 3.04; N, 29.14. $[Mn_9(2poap)_6]_2[Mn(NCS)_4(H_2O)]_2(NCS)_8\cdot 10H_2O$ (**2**). Anal. Calcd for $(C_{19}H_{15}N_9O_2)_{12}Mn_{18}(Mn(H_2O)(NCS)_4)_2(NCS)_8\cdot(H_2O)_{10}$: C, 41.50; H, 2.91; N, 24.60. Found: C, 41.26; H, 2.72; N, 25.12. $[Mn_9(2poapz)_6](NO_3)_6\cdot 14.5H_2O$ (**3**). Anal. Calcd for $(C_{17}H_{13}N_{11}O_2)_6Mn_9(NO_3)_6\cdot(H_2O)_{14.5}$: C, 34.49; H, 3.02; N, 28.42. Found: C, 34.47; H, 2.62; N, 28.85.[5] $[Mn_9(2poapz)_6](ClO_4)_6\cdot 10.5H_2O$ (**11**). Anal. Calcd for $(C_{17}H_{13}N_{11}O_2)_6Mn_9(ClO_4)_6\cdot(H_2O)_{10.5}$: C, 33.11; H, 2.68; N, 24.98. Found: C, 33.13; H, 2.39; N, 24.99.

$[Mn_9(Cl2poap)_6](ClO_4)_9\cdot 7H_2O$ (6) and $[Mn_9(Cl2poap)_6](ClO_4)_9\cdot 10H_2O$ (7). $[Mn_9(Cl2poap)_6](ClO_4)_6\cdot 10H_2O$ (**8**)[6] (0.080 g, 0.020 mmol) was dissolved in acetonitrile (20 mL) to give a deep red-orange solution. $NaClO_4$ (0.020 g) dissolved in water (3 mL) was added, followed by saturated chlorine water (12 mL). The solution became brown after several hours, and the solvent was allowed to evaporate slowly at room temperature. Dark brown crystals of **6** suitable for structural study were deposited after several days in almost quantitative yield. They were kept under mother liquor prior to structural analysis. Anal. Calcd for $(C_{19}H_{14}N_9O_2Cl)_6Mn_9(ClO_4)_9\cdot(H_2O)_7$: C, 33.15; H, 2.39; N, 18.31. Found: C, 32.68; H, 2.20; N, 18.33. **7** was prepared in a similar manner using saturated Br_2(aq), and also obtained as dark brown crystals. Anal. Calcd for $(C_{19}H_{14}N_9O_2Cl)_6Mn_9(ClO_4)_9\cdot(H_2O)_{10}$: C, 32.76; H, 2.49; N, 18.10. Found: C, 32.68; H, 2.20; N, 18.06.

$[Mn_9(S2poap)_6](ClO_4)_{10}\cdot 12H_2O$ (12). S2poap was added to a solution of an excess of $Mn(ClO_4)_2\cdot 6H_2O$ in acetonitrile, forming a red solution, which produced a red crystalline product after concentration to a small volume and addition of ether (yield 77%). The crystals were not suitable for a structural analysis. Anal. Calcd for $(C_{19}H_{15}N_9O_2S)_6Mn_9(ClO_4)_{10}\cdot(H_2O)_{12}$: C, 31.80; H, 2.67; N, 17.57. Found: C, 31.67; H, 2.64; N, 17.54.

Electrochemical Oxidation. Bulk electrochemical oxidation was carried out in a three-electrode cell comprising a platinum mesh working electrode (anode), platinum mesh counter electrode (cathode) in a separate compartment separated by a glass frit, and saturated Ag/AgCl reference electrode. **8** (0.280 g) and tetraethylammonium perchlorate (0.690 g) were dissolved in a mixture of acetonitrile (100 mL) and water (100 mL), forming a clear orange solution. A potential of ∼15 V was applied across the electrodes using an HP 6215A power supply, and 1 mL of 70% $HClO_4$(aq) was added to the counter electrode compartment. The potential was then adjusted to 1.8 ± 0.2 V with respect to the Ag/AgCl reference electrode and electrolysis was continued for 7 h with the formation of a brown solution, and evolution of hydrogen gas at the cathode. The solution was filtered and its volume reduced by evaporation under reduced pressure, with the formation of a dark brown crystalline solid, which was isolated by filtration and washing with ether (yield 70%). Anal. Calcd for $(C_{19}H_{14}N_9O_2Cl)_6Mn_9(ClO_4)_9\cdot(H_2O)_6$ (**9**): C, 33.29; H, 2.36; N, 18.39. Found: C, 33.32; H, 2.44; N, 18.38.

Safety note: Perchlorate complexes are potentially explosive, and should be handled in small quantities. No problems with the current complexes have been encountered so far.

Crystallographic Data and Refinement of the Structures. The diffraction intensities of an orange-red prismatic crystal of **5** were collected with graphite-monochromatized Mo Kα X-radiation (rotating anode generator) using a Bruker P4/CCD diffractometer at 193(1) K to a maximum 2θ value of 52.9°. The data were

Table 1. Summary of Crystallographic Data for **1**−**6**

	1	**2**	**3**	**4**	**5**	**6**
empirical formula	$C_{122}H_{134}N_{66}O_{32}Mn_9$	$C_{242}H_{233}N_{121}O_{50}S_{13}Mn_{20}$	$C_{105}H_{127}N_{71}O_{43}Mn_9$	$C_{186}H_{138}N_{46}O_{30}Mn_9$	$C_{126}H_{118}N_{42}O_{20}Cl_{10}Mn_{11}$	$C_{114}H_{98}N_{54}O_{55}Cl_{15}Mn_9$
mol wt	3531.27	7151.82	3566.05	3991.87	3499.44	4130.67
cryst syst	tetragonal	triclinic	triclinic	tetragonal	tetragonal	triclinic
space group	$P4_2/n$	$P\bar{1}$ (No. 2)	$P\bar{1}$ (No. 2)	$P4_12_12$ (No. 92)	$I\bar{4}$ (No. 82)	$P\bar{1}$
a/Å	21.568(1)	25.043(1)	18.1578(12)	20.279(1)	18.2700(5)	19.044(2)
b/ Å		27.413(1)	18.2887(12)			19.457(2)
c/Å	16.275(1)	27.538(2)	26.764(2)	54.873(6)	26.753(2)	23.978(3)
α/deg	90	91.586(2)	105.7880(12)	90	90	84.518(3)
β/deg	90	113.9200(9)	101.547(2)	90	90	81.227(3)
γ/deg	90	111.9470(8)	91.1250(11)	90	90	60.954(2)
V/Å^3	7570.6(7)	15667(1)	8353.6(8)	22566(2)	8929.8(5)	7674(2)
ρ_{calcd}/(g cm^{-3})	1.549	1.516	1.418	1.175	1.301	1.788
T/K	193(1)	193(1)	193(1)	193(1)	193(1)	193(1)
Z	2	2	2	4	2	2
μ/cm^{-1}	8.19	9.48	7.48	5.54	9.63	10.83
no. of reflns collected						
total, unique, R_{int}	49927, 7768, 0.067	78112, 63600, 0.038	42722, 31487, 0.052	125625, 23102, 0.115	24519, 9160, 0.030	37579, 30780, 0.061
obsd ($I > 2.00\sigma(I)$)	5821	63600	14527	15252	9160	11233
final R1, wR2[a]	0.096, 0.262	0.093,0.334	0.134,0.429	0.111,0.323	0.061,0.195	0.112,0.286

[a] $R1 = \sum[F_o| - F_c|/\sum|F_o|$, $wR2 = [\sum[w(F_o|^2 - F_c|^2)^2]/\sum[w(F_o|^2)^2]]^{1/2}$.

corrected for Lorentz and polarization effects. The structure was solved by direct methods.[20,21] All atoms except hydrogens were refined anisotropically. Hydrogen atoms were placed in calculated positions with isotropic thermal parameters set to 20% greater than those of their bonded partners, and were not refined. Neutral atom scattering factors[22] and anomalous-dispersion terms[23,24] were taken from the usual sources. All other calculations were performed with the teXsan[25] crystallographic software package using a PC computer. Crystal data collection and structure refinement for **1** (red-brown prisms), **2** (red prisms), **3** (red-brown prisms), **4** (red-brown prisms), and **6** (dark brown prisms) were carried out in a similar manner using Mo Kα X-radiation. Abbreviated crystal data for **1**−**6** are given in Table 1.

Refinements for **3**, **4**, and **6** were hampered by weak data sets, lattice disorder effects, and the presence of an abundance of disordered water molecules. For **6** all of the perchlorate ions in the asymmetric unit were refined as rigid groups, and several were refined as disordered. While the modeling of the ligands and the polymetallic, cationic grid structures proceeded smoothly in all cases, the final refinement values are unfortunately a little high, particularly for **3**. The details presented are the best obtained from the current data sets, which were collected at low temperature on a rotating anode instrument equipped with a CCD detector. It is unlikely that improved refinements would be obtained with data sets from other crystalline samples. The difficulty in refining these structures is associated in part with poor crystal quality, very large cells, lattice disorder effects, large numbers of lattice-trapped solvent molecules, and as a result crystal instability. Typically crystals must be stored under mother liquor prior to data collection, and require immediate freezing once coated with oil and removed from the mother liquor; otherwise crystal decomposition occurs.

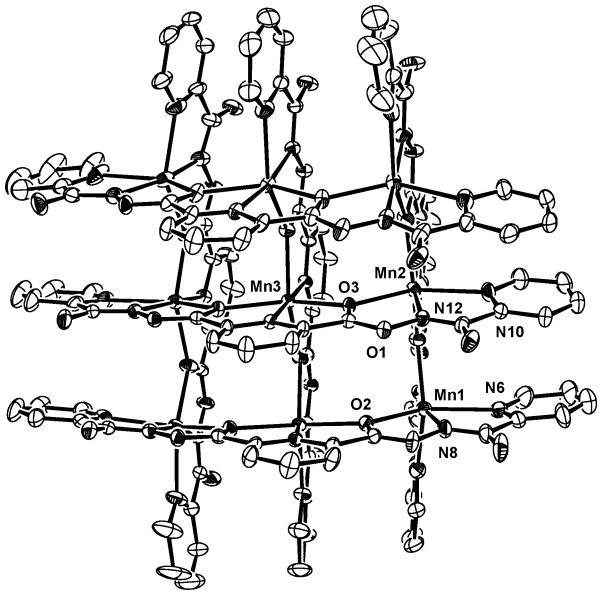

Figure 2. Structural representation of the cation in **1** (30% thermal ellipsoids).

Results and Description

Description of the Structures. The structure of the cation in **1** is shown in Figure 2, and important bond distances and angles are listed in Table 2. The tetragonal space group indicates 4-fold symmetry in the cation. The familiar homoleptic grid arrangement occurs with six roughly parallel heptadentate ligands arranged above and below the [Mn_9-(μ-O)$_{12}$] core, with the nine metal ions bridged by twelve alkoxide oxygen atoms within the core. Mn−Mn distances fall in the range 3.886−3.923 Å, with Mn−O−Mn angles in the range 126.7−126.93°, typical for grids in this class. Also by virtue of the symmetry in the grid the distances between corner Mn(II) centers are equal (7.770 Å). The corner Mn(II) centers have *cis*-MnN_4O_2 coordination environments, the side Mn(II) centers have *mer*-MnN_3O_3 coordination environments, and the center Mn(II) ion has a *trans*-

(19) Markees, D. G. *J. Org. Chem*. **1963**, *28*, 2530.
(20) (a) SHELX97: Sheldrick, G. M., 1997. (b) SIR97: Altomare, A.; Cascarano, M.; Giacovazzo, C.; Guagliardi, A *J. Appl. Crystallogr*. **1993**, *26*, 343.
(21) DIRDIF94: Beurskens, P. T.; Admiraal, G.; Beurskens, G.; Bosman, W. P.; de Gelder, R.; Israel, R.; Smits, J. M. M. *The DIRDIF-94 program system*; Technical Report of the Crystallography Laboratory; University of Nijmegen: Nijmegen, The Netherlands, 1994.
(22) Cromer, D. T.; Waber, J. T. *International Tables for X-ray Crystallography*; The Kynoch Press: Birmingham, England, 1974; Vol. IV, Table 2.2A.
(23) Ibers, J. A.; Hamilton, W. C. *Acta Crystallogr*. **1964**, *17*, 781.
(24) Creagh, D. C.; McAuley, W. J. In *International Tables for Crystallography*; Wilson, A. J. C., Ed.; Kluwer Academic Publishers: Boston, 1992; Vol. C, Table 4.2.6.8, pp 219−222.
(25) *teXsan for Windows: Crystal Structure Analysis Package*; Molecular Structure Corp., 1997.

Table 2. Bond Distances (Å) and Angles (deg) for **1**

Mn1	N3	2.147(6)	Mn2	O1	2.184(4)
Mn1	N8	2.165(7)	Mn2	O2	2.222(4)
Mn1	O2	2.169(4)	Mn2	N10	2.315(6)
Mn1	O1	2.196(4)	Mn3	N14	2.180(6)
Mn1	N1	2.296(7)	Mn3	O3	2.190(4)
Mn1	N6	2.319(7)	Mn1	Mn2	3.932 (2)
Mn2	N12	2.141(5)	Mn2	Mn3	3.886(2)
Mn2	O3	2.153(4)	Mn1	Mn2′	3.925(2)
Mn2	N5	2.181(5)			

Mn2	O1	Mn1	127.7(2)
Mn1	O2	Mn2	126.7(2)
Mn2	O3	Mn3	126.93(17)

MnN_2O_4 coordination environment. The central Mn atom has almost equal Mn−O and Mn−N distances (2.190(4) and 2.180(6) Å, respectively), and the corner Mn centers and the side Mn centers have much longer Mn−N distances to the external pyridine rings (2.319(7) and 2.215(2) Å, respectively), with shorter remaining Mn−N and Mn−O contacts (2.141−2.296 Å). The long external Mn−N distances are clearly a consequence of the stretching of the ligands over the nonanuclear core. The pyridine rings are arranged in an approximately parallel fashion with quite short inter-ring separations: 3.5−4.1 Å for the external rings and 3.3−3.7 Å for the central rings. This clearly indicates significant π interactions between the rings, and a stabilizing effect contributing to the self-assembly of the grid. The dicyanamide anions show no tendency to influence the stability of the grid, and are present as uncoordinated ions.

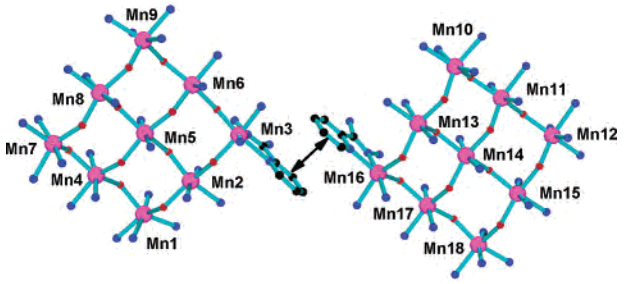

Figure 3. Core structure of **2** showing the two associated grids.

The structure of **2** is comprised of two $Mn(II)_9$ grids within the asymmetric unit, which are very close together, and linked by π interactions between two pyridine rings at the corners of two adjacent grid cations. The lattice contains many water molecules, five discernible thiocyanate anions, and two unusual trigonal-bipyramidal, five-coordinate $[Mn(H_2O)(NCS)_4]^{2-}$ anions. Important bond distances and angles are listed in Table 3. Fully labeled core structures for both Mn_9 cationic grid fragments are shown in Figures S1 and S2 (see the Supporting Information). Figure 3 shows the simplified core structures of the two cations (POVRAY), and the overlapping pyridine rings connecting Mn(3) and Mn(16), with inter-ring atom contacts falling in the range 3.455−3.960 Å. These short π interactions clearly indicate a way in which the grids can associate, which may lead to intergrid electronic and magnetic communication. Further examination of the extended structure of **2** shows that

Table 3. Bond Distances (Å) and Angles (deg) for **2**

Mn1	O12	2.160(6)	Mn6	N16	2.125(8)	Mn11	N93	2.123(7)	Mn16	N75	2.137(7)
Mn1	N3	2.164(7)	Mn6	N50	2.156(8)	Mn11	N59	2.176(7)	Mn16	N88	2.166(7)
Mn1	N30	2.169(7)	Mn6	O3	2.159(5)	Mn11	O21	2.180(5)	Mn16	O20	2.190(6)
Mn1	O6	2.199(5)	Mn6	O11	2.173(6)	Mn11	O13	2.194(6)	Mn16	O17	2.218(6)
Mn1	N28	2.281(8)	Mn6	O10	2.215(5)	Mn11	O14	2.231(6)	Mn16	N73	2.284(7)
Mn1	N1	2.319(7)	Mn6	N18	2.282(8)	Mn11	N91	2.407(7)	Mn16	N90	2.294(8)
Mn2	N39	2.128(7)	Mn7	N21	2.163(7)	Mn12	N102	2.146(7)	Mn17	N97	2.148(7)
Mn2	O8	2.166(5)	Mn7	N34	2.181(7)	Mn12	N61	2.160(7)	Mn17	O22	2.160(5)
Mn2	N5	2.177(7)	Mn7	O7	2.194(6)	Mn12	O14	2.182(6)	Mn17	N77	2.183(7)
Mn2	O1	2.189(6)	Mn7	O4	2.198(6)	Mn12	O23	2.188(5)	Mn17	O17	2.201(5)
Mn2	O12	2.204(5)	Mn7	N19	2.314(8)	Mn12	N63	2.323(8)	Mn17	O18	2.274(5)
Mn2	N37	2.299(7)	Mn7	N36	2.318(7)	Mn12	N100	2.399(7)	Mn17	N99	2.277(7)
Mn3	N48	2.136(8)	Mn8	N43	2.146(7)	Mn13	N66	2.142(7)	Mn18	N79	2.145(8)
Mn3	N7	2.161(8)	Mn8	O9	2.169(6)	Mn13	N86	2.169(7)	Mn18	N106	2.149(7)
Mn3	O10	2.190(6)	Mn8	N23	2.191(7)	Mn13	O15	2.176(5)	Mn18	O18	2.160(5)
Mn3	O1	2.212(6)	Mn8	O4	2.198(6)	Mn13	O20	2.198(6)	Mn18	O24	2.211(5)
Mn3	N9	2.309(8)	Mn8	O5	2.230(6)	Mn13	O19	2.223(6)	Mn18	N108	2.286(7)
Mn3	N46	2.369(7)	Mn8	N45	2.317(7)	Mn13	N64	2.318(7)	Mn18	N81	2.346(7)
Mn4	N12	2.142(7)	Mn9	N25	2.147(7)	Mn14	N68	2.172(7)	Mn19	N111	2.096(10)
Mn4	O2	2.152(6)	Mn9	N52	2.160(7)	Mn14	N95	2.178(7)	Mn19	N112	2.097(10)
Mn4	O6	2.193(6)	Mn9	O5	2.184(6)	Mn14	O22	2.200(5)	Mn19	N110	2.116(9)
Mn4	N32	2.198(7)	Mn9	O11	2.204(6)	Mn14	O16	2.211(6)	Mn19	N109	2.191(10)
Mn4	O7	2.230(6)	Mn9	N54	2.313(7)	Mn14	O21	2.231(5)	Mn19	O25	2.273(9)
Mn4	N10	2.341(8)	Mn9	N27	2.353(7)	Mn14	O15	2.243(5)	Mn20	N121	1.955(2)
Mn5	O2	2.170(6)	Mn10	N57	2.150(8)	Mn15	N70	2.148(7)	Mn20	N122	2.041(2)
Mn5	O9	2.170(5)	Mn10	N84	2.153(8)	Mn15	N104	2.184(7)	Mn20	N114	2.066(11)
Mn5	N41	2.172(7)	Mn10	O19	2.180(6)	Mn15	O16	2.192(5)	Mn20	N115	2.077(11)
Mn5	N14	2.172(6)	Mn10	O13	2.184(6)	Mn15	O24	2.201(5)	Mn20	O26	2.175(17)
Mn5	O8	2.209(5)	Mn10	N55	2.320(9)	Mn15	O23	2.243(5)			
Mn5	O3	2.211(6)	Mn10	N82	2.368(7)	Mn15	N72	2.377(7)			

Mn2	O1	Mn3	129.0(3)	Mn8	O9	Mn5	127.2(3)	Mn17	O17	Mn16	128.9(3)
Mn4	O2	Mn5	129.3(3)	Mn3	O10	Mn6	127.9(3)	Mn18	O18	Mn17	128.2(3)
Mn6	O3	Mn5	127.2(3)	Mn6	O11	Mn9	127.8(3)	Mn10	O19	Mn13	129.1(3)
Mn7	O4	Mn8	128.0(3)	Mn1	O12	Mn2	125.7(2)	Mn16	O20	Mn13	127.8(3)
Mn9	O5	Mn8	129.1(3)	Mn10	O13	Mn11	127.9(3)	Mn11	O21	Mn14	130.3(3)
Mn4	O6	Mn1	128.0(3)	Mn12	O14	Mn11	127.0(3)	Mn17	O22	Mn14	126.9(3)
Mn7	O7	Mn4	126.7(3)	Mn13	O15	Mn14	128.1(2)	Mn12	O23	Mn15	131.1(3)
Mn2	O8	Mn5	126.9(3)	Mn15	O16	Mn14	128.9(3)	Mn15	O24	Mn18	128.0(3)

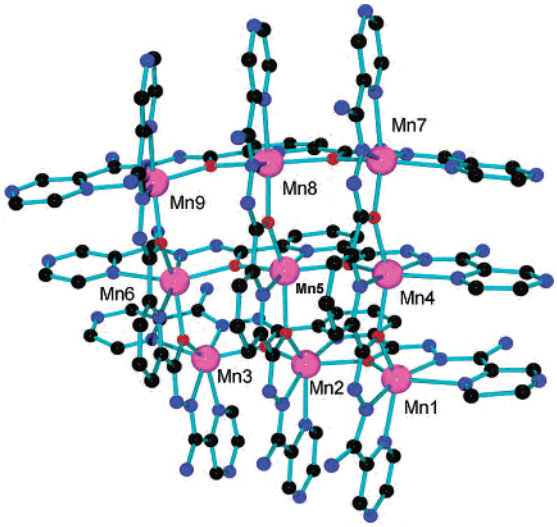

Figure 4. Structural representation of the cation in **3** (30% thermal ellipsoids, POVRAY format).

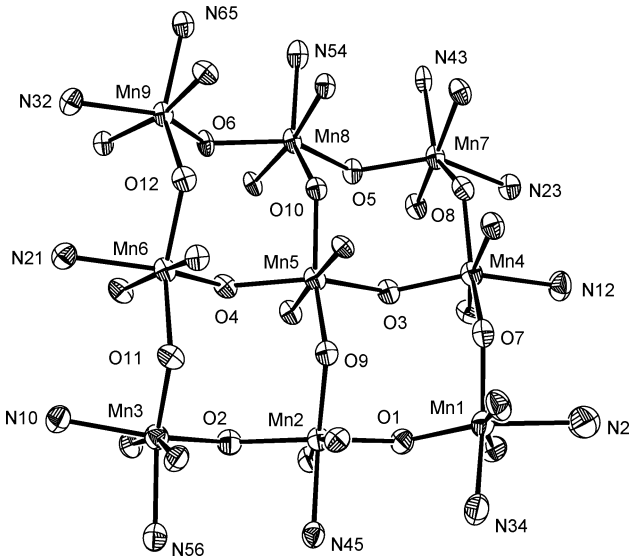

Figure 5. Core structure of **3**.

Mn(7) and Mn(12) are also connected by a similar π interaction, with cross ring contacts as short as 3.55 Å. An extended structural representation showing Mn(3)−Mn(16) and Mn(7)−Mn(12) contacts is available in Figure S3 (see the Supporting Information). The grids are effectively connected in associated chains in the *xy* plane (Mn(3)−Mn(16) = 9.069 Å, Mn(7)−Mn(12) = 8.907Å). Mn−Mn distances within each grid fall in the normal range (3.882−4.034 Å), and Mn−O−Mn angles in the range 125.7−131.1°. The two grid cations resemble closely the structure of the grid in **1**, with the same ligand. The charge balance clearly requires three additional thiocyanate anions (eight indicated from the elemental analysis), and these are presumably lost among the "solvent" peaks assigned in the lattice. Given the very complex nature of the system, and the less than ideal level of the refinement of the structure, it is reasonable to assume that some lattice fragments remain unidentified.

The molecular structure of the cation in **3** is shown in Figure 4 (POVRAY), and important bond distances and angles are listed in Table 4. The core structure is shown in Figure 5, with just the immediate donor atoms. The overall grid structure is very similar to that in **1** and **2**. Mn−Mn distances fall in the range 3.902−3.941 Å, with Mn−O−Mn angles in the range 127.0−128.7°. The presence of terminal pyrazine rings leads to somewhat longer external Mn−N distances (2.302−2.502 Å) than those found for **1** and **2**, in keeping with the weaker donor character of pyrazine compared with pyridine. The overall core dimensions are essentially the same as those in **1** and **2** (Mn−Mn corner distances 7.722−7.771 Å).

The structure of the cation in **4** is shown in Figure 6 (POVRAY), and important bond distances and angles are listed in Table 5. The core structure, showing just the metal ions and ligands, is shown in Figure 7 (POVRAY). What is immediately apparent in the structure is the steric crowding at the ends of each 2popp ligand, which has both pyridine and phenyl rings bonded to the terminal carbon of the ligand backbone. The pyridine rings are coordinated in their usual way, with the aromatic rings forming the typical π-stacked

Table 4. Bond Distances (Å) and Angles (deg) for **3**

Mn1	N4	2.110(13)	Mn5	O10	2.194(7)
Mn1	N37	2.142(11)	Mn5	O3	2.198(7)
Mn1	O1	2.159(8)	Mn5	O9	2.226(7)
Mn1	O7	2.174(8)	Mn6	N19	2.151(8)
Mn1	N34	2.362(12)	Mn6	O4	2.159(7)
Mn1	N2	2.502(2)	Mn6	N61	2.169(8)
Mn2	O9	2.140(7)	Mn6	O12	2.197(7)
Mn2	N48	2.164(8)	Mn6	O11	2.228(7)
Mn2	N6	2.198(9)	Mn6	N21	2.381(10)
Mn2	O2	2.203(8)	Mn7	N41	2.111(9)
Mn2	O1	2.219(8)	Mn7	O5	2.157(7)
Mn2	N45	2.405(10)	Mn7	N26	2.160(9)
Mn3	N59	2.108(10)	Mn7	O8	2.181(8)
Mn3	O11	2.151(7)	Mn7	N23	2.315(9)
Mn3	O2	2.157(8)	Mn7	N43	2.372(10)
Mn3	N8	2.177(10)	Mn8	N52	2.120(8)
Mn3	N56	2.346(10)	Mn8	O10	2.147(7)
Mn3	N10	2.348(11)	Mn8	N28	2.179(7)
Mn4	N15	2.127(9)	Mn8	O5	2.190(7)
Mn4	O3	2.137(7)	Mn8	O6	2.213(7)
Mn4	N39	2.161(9)	Mn8	N54	2.378(10)
Mn4	O7	2.170(8)	Mn9	N63	2.147(8)
Mn4	O8	2.190(7)	Mn9	N30	2.149(8)
Mn4	N12	2.367(11)	Mn9	O6	2.150(6)
Mn5	N50	2.169(7)	Mn9	O12	2.152(7)
Mn5	N17	2.181(8)	Mn9	N65	2.301(9)
Mn5	O4	2.184(7)	Mn9	N32	2.347(9)

Mn1	O1	Mn2	128.3(4)	Mn4	O7	Mn1	128.4(4)
Mn3	O2	Mn2	127.0(3)	Mn7	O8	Mn4	127.9(3)
Mn4	O3	Mn5	128.5(3)	Mn2	O9	Mn5	128.6(3)
Mn6	O4	Mn5	128.2(3)	Mn8	O10	Mn5	128.7(3)
Mn7	O5	Mn8	127.7(3)	Mn3	O11	Mn6	128.3(3)
Mn9	O6	Mn8	127.5(3)	Mn9	O12	Mn6	127.2(3)

arrangement. Inter-ring distances between equivalent ring atoms on pyridine rings bonded to Mn(1) and Mn(4) fall in the range 3.81−3.92 Å, while for Mn(4) and Mn(6) the distances are in the range 3.65−4.20 Å. However, the phenyl rings are arranged in a similar stack, but are not as parallel. Equivalent inter-ring distances for phenyl rings close to Mn(1), Mn(4), and Mn(6) are in the ranges 4.05−4.72 and 4.00−5.13 Å, respectively. Similar inter-ring distances are observed for the Mn(1), Mn(2), and Mn(3) groupings.

The effect of the steric crowding is to exert a major distortion on the grid as a whole, with compression of the "square" along the Mn(3)−Mn(5)−Mn(6) axis forming a

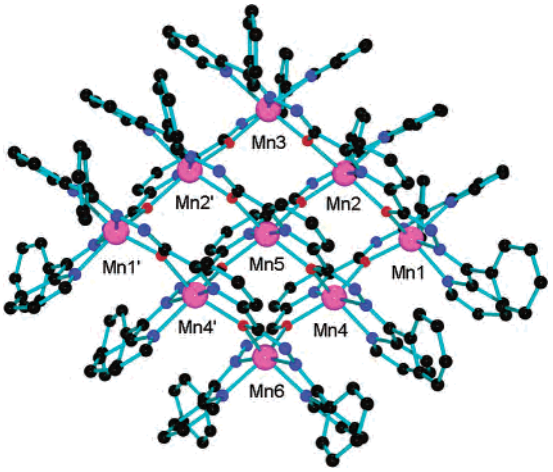

Figure 6. Structural representation of the cation in **4** (30% thermal ellipsoids, POVRAY format).

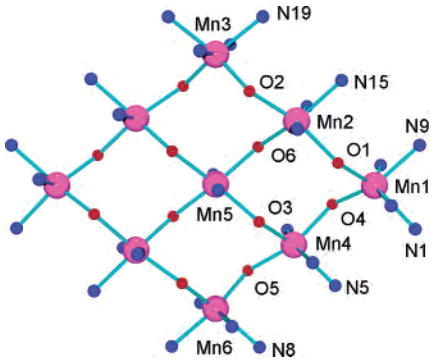

Figure 7. Core structure of **4**.

Table 5. Bond Distances (Å) and Angles (deg) for **4**

Mn1	O1	2.155(6)	Mn4	O3	2.150(6)
Mn1	O4	2.169(6)	Mn4	N12	2.160(7)
Mn1	N2	2.174(8)	Mn4	O5	2.210(6)
Mn1	N10	2.177(8)	Mn4	N6	2.220(7)
Mn1	N9	2.292(8)	Mn4	O4	2.229(6)
Mn1	N1	2.300(8)	Mn4	N5	2.273(8)
Mn2	O6	2.175(6)	Mn5	N18	2.159(6)
Mn2	N4	2.180(7)	Mn5	N18	2.159(6)
Mn2	N16	2.233(7)	Mn5	O3	2.231(6)
Mn2	O1	2.246(6)	Mn5	O3	2.231(6)
Mn2	O2	2.253(6)	Mn5	O6	2.233(6)
Mn2	N15	2.278(7)	Mn5	O6	2.233(6)
Mn3	O2	2.163(6)	Mn6	O5	2.174(6)
Mn3	O2	2.163(6)	Mn6	O5	2.174(6)
Mn3	N20	2.182(7)	Mn6	N14	2.184(8)
Mn3	N20	2.182(7)	Mn6	N14	2.184(8)
Mn3	N19	2.272(8)	Mn6	N8	2.270(8)
Mn3	N19	2.272(8)			

Mn1	O1	Mn2	128.0(3)	Mn1	O4	Mn4	125.6(3)
Mn3	O2	Mn2	127.3(3)	Mn6	O5	Mn4	125.7(3)
Mn4	O3	Mn5	128.0(3)	Mn2	O6	Mn5	127.4(3)

diamond-shaped grid. Mn(1)−Mn(6) and Mn(1)−Mn(3) distances are normal (7.727 and 7.850 Å, respectively), but the Mn(3)−Mn(6) distance (9.799 Å) is much shorter than the Mn(1)−Mn(1)′ distance (12.11 Å). This is in sharp contrast to the other Mn_9 systems, which have approximately square, but twisted core arrangements, and indicates a subtle way of changing the overall grid dimensions. Individual Mn−Mn separations (3.90−3.96 Å) and Mn−O−Mn angles (126.0−128.3°) are normal. It is of interest to note also that

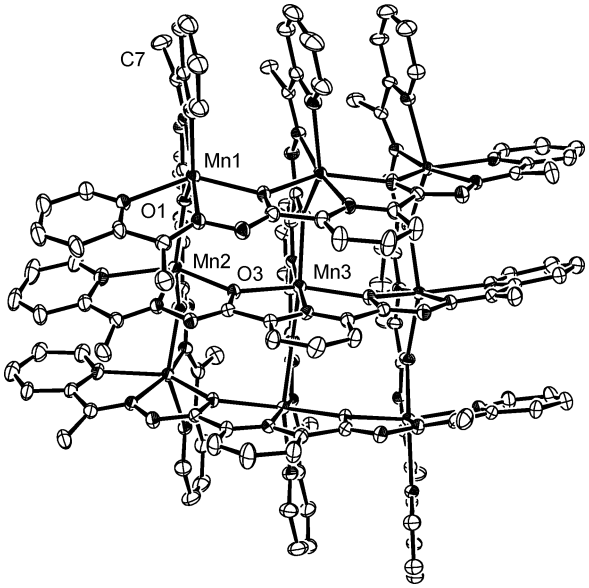

Figure 8. Structural representation of the cation in **5** (30% thermal ellipsoids).

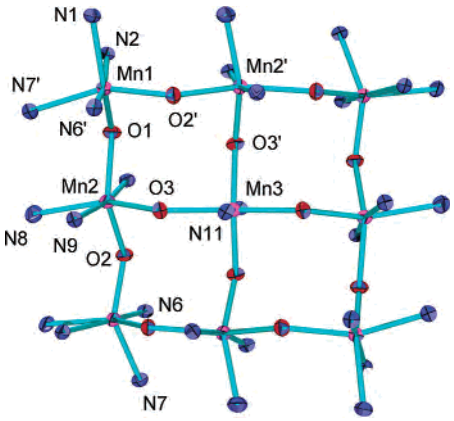

Figure 9. Core structure of **5**.

Table 6. Bond Distances (Å) and Angles (deg) for **5**

Mn1	O1	2.172(4)	Mn2	N8	2.286(5)
Mn1	N6	2.172(5)	Mn3	N11	2.180(6)
Mn1	O2	2.181(3)	Mn3	O3	2.199(3)
Mn1	N2	2.196(5)	Mn4	Cl1	2.3674(14)
Mn1	N7	2.256(4)	Mn4	Cl1	2.3674(14)
Mn1	N1	2.286(4)	Mn4	Cl1	2.3675(14)
Mn2	O3	2.153(3)	Mn4	Cl1	2.3675(14)
Mn2	N9	2.176(5)	Mn5	Cl2	2.3647(19)
Mn2	N4	2.180(5)	Mn5	Cl2	2.3647(19)
Mn2	O2	2.200(3)	Mn5	Cl2	2.3648(19)
Mn2	O1	2.230(3)	Mn5	Cl2	2.3648(19)

Mn1	O1	Mn2	128.52(18)	Mn2	O3	Mn3	127.64(16)
Mn1	O2	Mn2	128.38(18)				

Mnligand distances in **4** do not exceed 2.3 Å, contrary to what is observed in most other $Mn(II)_9$ grids.

The structure of the cation in **5** is shown in Figure 8, and important bond distances and angles are listed in Table 6. The structural core showing the metal ions, with the immediate ligand atoms, is shown in Figure 9 (POVRAY). Mn−Mn distances fall in the range 3.90−3.97 Å, and Mn−O−Mn angles in the range 127.6−128.6°, with a corner to corner metal separation of 7.824 Å. The ligand 2pomp has a methyl group bonded to the terminal carbon of the ligand

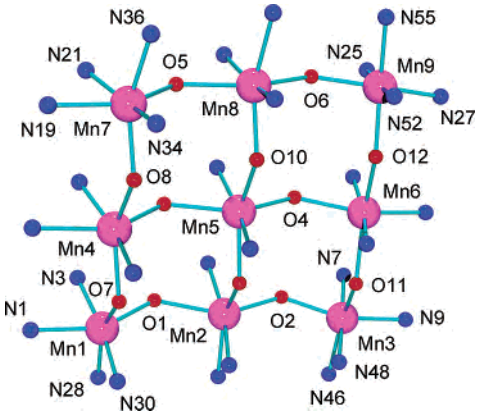

Figure 10. Core structure of **6**.

backbone, and unlike 2popp there is no significant steric effect associated with this group leading to any distortion of the grid. In this respect it behaves like the parent ligand 2poap. Metal−ligand distances are typical for the Mn grids.

Compound **6** is derived by chemical oxidation of the complex $[Mn_9(Cl2poap\text{-}2H)_6](ClO_4)_6 \cdot 8H_2O$ (**8**)[6] with chlorine. The complex formed as dark brown needles in high yield, but a weak data set and difficulties with the solution, due in part to disorder in the lattice perchlorates, and with one pyridine ring, bound to Mn(9), which is disordered over two ring positions, led to a less than ideal solution. However, the grid is clearly defined, and the number of perchlorate anions in the lattice can be reasonably estimated in agreement with the elemental analysis. The core structure is shown in Figure 10 (POVRAY). Adjacent Mn−Mn distances fall in the range 3.87−4.03 Å, and Mn−Mn distances between corner metals fall in the range 7.80−7.99 Å, similar to the other square $Mn(II)_9$ grids (Table 7). The most relevant comparison grid is **8**,[6] which has adjacent Mn−Mn distances in the range 3.886−4.055 Å, and corner Mn−Mn distances of 7.720−8.051 Å, overall dimensions very similar to those of **6**. However, close examination of Mn−ligand distances for **6** reveals some rather short contacts to three of the corner metal ions, Mn(1), Mn(3), and Mn(9) (average 2.066, 2.055, and 2.062 Å, respectively), much shorter than would be anticipated for Mn(II) ions, but consistent with Mn(III) centers. The average Mn−L distance of 2.164 Å for Mn(7) suggests that this site is mostly Mn(II). Comparable Mn−L distances for the corner manganese sites in **8** are in the range 2.122−2.388 Å, with average values of 2.213, 2.210, 2.229, and 2.226 Å.

Jahn−Teller distortions would be expected for Mn(1), Mn(3), and Mn(9), but despite two quite short distances in each case (<2 Å), defining such a distortion is not obvious. Metal centers in the grids are in general highly distorted anyway, regardless of the metal and its oxidation state, and this is due in large measure to the balance of metal−ligand donor interactions, and packing constraints of the ligands as they assemble around the core. However, the longest axes can be defined as N(1)−Mn(1)−O(1), N(46)−Mn(3)−O(11), and N(55)−Mn(9)−O(12) for the Mn(III) centers, which may be considered as the Jahn−Teller axes. The Mn−O−Mn angles for **6** fall in the range 129.6−135.2°, which is considerably larger than similar angles observed in the parent $Mn(II)_9$ grid complex **8** (126.4−130.7°). The larger angles are associated with Mn(1), Mn(3), and Mn(9), again an indication that these are the Mn centers which are oxidized. This can be reasonably rationalized in terms of an overall grid dimension that is essentially unchanged compared with that of the parent complex **8**,[6] but with shorter overall bond distances within the outer ring of eight Mn centers involving Mn(1), Mn(3), and Mn(9). The disorder in the structure, and the difficulty of fixing the occupancy of some perchlorates, points to the possibility of different grids within the lattice, in terms of the Mn(II) and Mn(III) site composition. However, it is quite clear that at least three Mn centers on average in **6** are in the 3+ oxidation state.

Table 7. Bond Distances (Å) and Angles (deg) for **6**

Mn1	N30	1.947(8)	Mn5	O4	2.253(9)
Mn1	N3	1.971(9)	Mn5	O3	2.256(9)
Mn1	O7	2.031(6)	Mn6	N16	2.079(9)
Mn1	N28	2.092(8)	Mn6	N50	2.144(9)
Mn1	O1	2.150(8)	Mn6	O4	2.159(8)
Mn1	N1	2.204(11)	Mn6	O12	2.237(8)
Mn2	N39	2.095(8)	Mn6	N18	2.255(14)
Mn2	N5	2.164(8)	Mn6	O11	2.257(7)
Mn2	O9	2.184(7)	Mn7	N34	2.073(9)
Mn2	O2	2.220(8)	Mn7	N21	2.075(12)
Mn2	O1	2.227(8)	Mn7	O8	2.129(8)
Mn2	N37	2.279(8)	Mn7	O5	2.160(10)
Mn3	N7	1.943(10)	Mn7	N36	2.245(9)
Mn3	N48	1.962(9)	Mn7	N19	2.301(15)
Mn3	O2	2.030(8)	Mn8	N43	2.092(9)
Mn3	O11	2.075(7)	Mn8	O10	2.170(7)
Mn3	N9	2.143(11)	Mn8	N23	2.178(10)
Mn3	N46	2.176(9)	Mn8	O5	2.268(11)
Mn4	N12	2.129(9)	Mn8	O6	2.293(11)
Mn4	O3	2.175(9)	Mn8	N45	2.369(10)
Mn4	N32	2.188(8)	Mn9	N25	1.961(13)
Mn4	O8	2.211(7)	Mn9	N52	1.978(11)
Mn4	O7	2.249(6)	Mn9	O6	2.045(11)
Mn4	N10	2.379(12)	Mn9	O12	2.125(7)
Mn5	N14	2.197(8)	Mn9	N55	2.126(16)
Mn5	N41	2.200(7)	Mn9	N27	2.139(18)
Mn5	O9	2.220(7)	Mn9	N54	2.329(19)
Mn5	O10	2.230(7)			

Mn1	O1	Mn2	133.8(3)	Mn1	O7	Mn4	132.2(3)
Mn3	O2	Mn2	131.2(3)	Mn7	O8	Mn4	130.0(3)
Mn4	O3	Mn5	130.0(3)	Mn2	O9	Mn5	129.4(3)
Mn6	O4	Mn5	130.0(3)	Mn8	O10	Mn5	131.0(3)
Mn7	O5	Mn8	129.7(4)	Mn3	O11	Mn6	134.3(3)
Mn9	O6	Mn8	134.3(3)	Mn9	O12	Mn6	135.1(4)

Electrochemical Properties and Chemical and Electrochemical Oxidation of $Mn(II)_9$ Grids. The cyclic voltammetry of an acetonitrile solution of **8** is shown in Figure 11. A prominent quasi-reversible wave occurs at $E_{1/2}$ = 0.73 V (ΔE_p = 216 mV), which has been shown to correspond to a four-electron redox process using controlled potential electrolysis, and assigned to the oxidation of four Mn(II) centers to Mn(III). Three less distinct waves occurring at higher potentials ($E_{1/2}$ = 1.16 V (ΔE_p = 116 mV), 1.33 V (ΔE_p = 102 mV), and 1.54 V (ΔE_p = 76 mV)) each correspond to one-electron redox processes (CPE), and are associated with oxidation of three other Mn(II) centers to Mn(III). The closely related complex $[Mn_9(2poap)_6](ClO_4)_6 \cdot 18H_2O$ (**10**) shows similar electrochemical behavior,[1] with a broad, quasi-reversible four-electron wave at $E_{1/2}$ = 0.69 V (ΔE_p = 144 mV), and four discernible one-electron waves

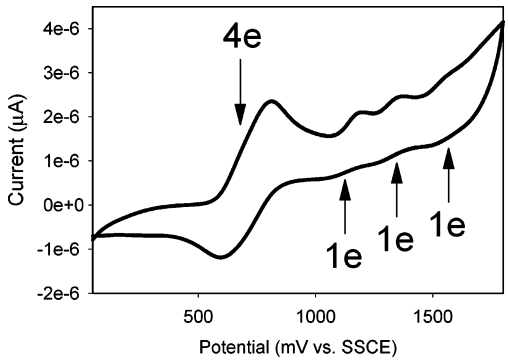

Figure 11. Cyclic voltammetry for **8** (CH_3CN, 1.0 mM, TEAP (0.1 M), Ag/AgCl).

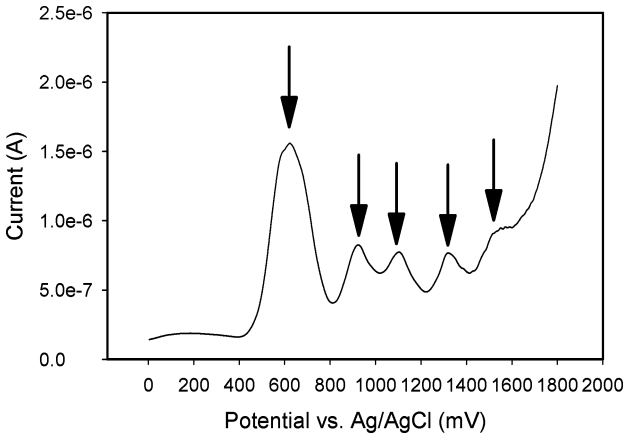

Figure 12. Differential pulse voltammetry for **8** (CH_3CN, 1.0 mM, TEAP (0.1 M), Ag/AgCl), using a 20 mV/s scan rate, 50 mV pulse amplitude, and 50 ms pulse width.

at $E_{1/2} = 1.00$ V ($\Delta E_p = 106$ mV), 1.18 V ($\Delta E_p = 116$ mV), 1.36 V ($\Delta E_p = 96$ mV), and 1.53 V ($\Delta E_p = 92$ mV), again associated with Mn(II) to Mn(III) oxidations. The shift to slightly higher potentials for **8** is reasonably associated with the presence of the electron-withdrawing chlorine atoms on the central pyridine rings in the ligand Cl2poap. The similar broad four-electron process observed for both compounds around 0.7 V is associated with oxidation of four Mn(II) centers which are fairly remote electronically, in the sense that when one is oxidized the oxidation potential of the next metal does not change significantly (the broad nature of this wave may indicate that there is slight communication between these metal centers, and that successive oxidation couples occur at slightly different potentials). The corner metal sites would reasonably fit this requirement (vide infra). The remaining one-electron redox waves occur at successively higher potentials, suggesting some communication between the metal ions. The side metal ions can reasonably communicate electronically through the central Mn(II), and are assigned to these waves. It is of interest to note that the four corner metal ions have MnN_4O_2 coordination environments, while the side metal ions have MnN_3O_3 coordination spheres, which might have suggested the opposite assignment.

Differential pulse voltammetry reveals features associated with the individual redox steps in **8** much more clearly, as shown in Figure 12. Five waves show up, with some resolution of the large first wave at 630 mV (note that the reference electrode is Ag/AgCl in this case). This indicates that the first four electrons are probably not lost in a concerted process.

In an attempt to isolate mixed-oxidation-state species, and check the assignment of metal site oxidation, a chemical oxidation approach was attempted in which the oxidation potential of a chemical oxidant was "matched" against a particular redox wave. Cl_2(aq) ($E_0 = 1.36$ V) and Br_2(aq) ($E_0 = 1.07$ V) were selected to probe the oxidation chemistry associated with the first four-electron wave only. **8** was reacted in aqueous acetonitrile with Cl_2(aq) and Br_2(aq) in the presence of added $NaClO_4$. However, since nonstandard conditions prevail in saturated aqueous solutions of Cl_2 and Br_2, the actual potentials will be slightly different. The change in color of the solution from red-orange to dark brown, on reaction with halogen (see the Experimental Section), is accompanied by the appearance of broad, fairly intense bands in the visible spectrum at 700 and 1000 nm ($\epsilon = 400-500$ M^{-1} cm^{-1}), which are assigned to intervalence charge transfer, and clearly support oxidation of some Mn(II) centers. A detailed analysis of the charge-transfer spectra of a number of Mn(II)/Mn(III) mixed-oxidation-state grids will appear elsewhere.[17] The isolation of **6** (vide ante) and **7**, and the structural solution for **6**, shows that the broad wave at ~0.7 V is associated with oxidation of the corner Mn(II) centers to Mn(III), as predicted. It is not immediately clear why only three metal ions have been oxidized, despite the use of excess oxidant in the case of both Cl_2 and Br_2, but the increasing cationic charge accompanying successive oxidation steps will clearly affect the successive equilibrium steps in the overall oxidation process. Other chemical oxidants, e.g., Ce(IV), OXONE, $KMnO_4$, and $K_2Cr_2O_7$, were tried, but a clean reaction was obtained only with Ce(IV), producing brown crystals, which were unsuitable for a structural determination.

Bulk electrolysis (vide ante), however, has proven to be a method for cleanly oxidizing the grids, and using a potential of ~1.8 V (vs Ag/AgCl) in a three-electrode cell with a solution of **8** in aqueous acetonitrile has produced the complex $[Mn_9(Cl2poap)](ClO_4)_9 \cdot 6H_2O$ (**9**), which appears to be identical to **6** and **7** (identical infrared spectra, good elemental analysis), with the oxidation of just three Mn(II) centers. Applying potentials in this range appears not to produce a four-electron-oxidized species, and larger voltages may be required. Further experiments are under way to examine the redox behavior of **8** and **10** at much larger applied potentials.

The complex $[Mn_9(2poapz)_6](ClO_4)_6 \cdot 10.5H_2O$ (**11**), which has the same grid cation as that found in **3**, exhibits three clearly defined waves (CH_3CN, 2.4×10^{-4} M, 0.1 M TEAP, scan rate 65 mV/s, vs SSCE) at $E_{1/2} = 0.86$ V (four electrons from CPE), $E_{1/2} = 1.29$ V (one electron), and $E_{1/2} = 1.47$ V (one electron). The significant positive shifts in these waves compared with those for **10** is clearly associated with the presence of terminal pyrazine rings rather than pyridine rings, which are somewhat weaker donors, and would tend to make the metal ions more electropositive. Cyclic voltammetry on

4 in acetonitrile shows similar regions of electrochemical activity, but with poorly defined redox waves overall. This can perhaps be attributed to the highly distorted nature of this complex. Compound **5** was not soluble enough in acetonitrile to study its electrochemistry, and a solution in DMSO showed no electrochemical response.

Magnetic Properties of the Manganese Grids. In general the $Mn(II)_9$ grids exhibit magnetic properties which are dominated by intramolecular antiferromagnetic exchange coupling, with room temperature magnetic moments in the range 16−17 μ_B, dropping to around 6 μ_B at 2 K (vide infra). The magnetic ground state has been shown to be $S = 5/2$ in the case of **10**, with the antiferromagnetic exchange coupling in the outer ring of eight Mn(II) centers dominating the exchange situation (Figure 1; $J \gg J'$).[4] Magnetization studies as a function of field have shown that upper excited states in the complex spin manifold are populated with increasing field beginning at ∼3 T, and torque studies have shown a field-induced level crossing at ∼7.5 T, accompanied by an abrupt change of magnetic anisotropy from easy-axis to hard-axis type.[4] A similar high-field population of upper excited states has been observed for the linear trinuclear complex $[Mn_3(CH_3COO)_6\ (bpy)_2]$, where the spin level crossover occurs at much higher field (∼10 T).[26]

$$H = -J(\sum_{i=1-7} S_i S_{i+1} + S_8 S_1) - J'(S_2 + S_4 + S_6 + S_8)S_9 \quad (1)$$

Assuming an idealized [3 × 3] grid structure, the isotropic nearest neighbor exchange terms are represented by the exchange Hamiltonian shown in eq 1 (see Figure 1). J is the exchange coupling constant within the eight-membered outer ring, and J' the exchange coupling constant between the central Mn atom and its immediate neighbors (dipole−dipole, second-order ligand field, and Zeeman terms are ignored). Solving the isotropic exchange problem for a grid of this size with 45 spins and two J values (Figure 1) is beyond the ability of any PC computer, and even most mainframe systems, unless symmetry elements are imposed on the spin vector coupling scheme. Even imposing, e.g., spin rotational and D_4 spin permutational symmetry, the matrix diagonalization problem is too large to calculate the total spin-state combinations and their energies (largest dimension 22210) using the average PC. However, a simpler alternative approach is to consider the outer ring of eight Mn(II) centers as an isolated chain (reasonable for a chain length of eight spin centers), and assume that there is effectively no coupling between the ring (chain) and the central Mn(II) ion, a model consistent with earlier studies.[4] This can be accomplished using the Fisher model (eqs 2 and 3)

$$\chi_{Mn} = \frac{Ng^2\beta^2 S(S+1)}{3kT}\frac{(1+u)}{(1-u)} \quad (2)$$

$$u = \coth\left[\frac{JS(S+1)}{kT}\right] - \left[\frac{kT}{JS(S+1)}\right] \quad (3)$$

$$\chi_{mol} = [(8\chi_{Mn} + 1.094g^2)/(T - \Theta)](1 - \alpha) + (1.094g^2/T)\alpha + \mathrm{TIP} \quad (4)$$

for an $S = 5/2$ chain,[27] where the large local spin ($S = 5/2$) is treated as a classical vector. Figure 13 illustrates the profile of magnetic moment per mole as a function of temperature for compound **1**. The data were fitted to eqs 2−4, with the susceptibility scaled for eight spin-coupled Mn(II) centers, and corrected for temperature-independent paramagnetism (TIP), the paramagnetic impurity fraction (α), intermolecular exchange effects (Θ = Weiss-like temperature correction), and the central, "isolated" Mn(II) center (eq 4). An excellent data fit gave $g = 2.028$, $J = -4.7$ cm^{-1}, $\alpha = 0.001$, TIP = 0 emu·mol^{-1}, and $\Theta = 0$ K ($10^2R = 1.9$; $R = [\sum(\chi_{obsd} - \chi_{calcd})^2/\sum\chi_{obsd}^2]^{1/2}$). The solid line in Figure 13 was calculated with these parameters. The accurate reproduction of the data over the whole temperature range indicates that the chain model is reasonable down to 2 K, and that $J \gg J'$. A spin model for the grid, and others in this class, is shown in Figure 14, with an alternation of Mn(II) $S = 5/2$ dipoles around the ring (chain) creating an effective $S = 0$ ground state at low temperatures, thus resulting in an $S = 5/2$ ground state overall when the central manganese atom is included. This result is in complete agreement with earlier studies on compound **10**.[4]

The magnetic properties of **2** combine two grid cations and two mononuclear anionic Mn(II) species. The magnetic moment per mole drops smoothly from 25.0 μ_B at 300 K to 11.5 μ_B at 2 K (overall profile similar to that of **1**), indicating intramolecular antiferromagnetic exchange within the grids. The data were fitted to eqs 2−4, suitably adapted for two grids and two isolated monuclear Mn(II) anions to give $g_{av} = 1.992$, $J = -4.7$ cm^{-1}, $\alpha = 0.001$, TIP = 0 emu·mol^{-1}, and $\Theta = -1$ K ($10^2R = 2.8$) (see Figure S4). The moment value at 2 K is consistent with the presence of two isolated Mn(II) centers, and two grids with the expected $S = 5/2$ ground states ($\mu_{calcd} = 11.9\ \mu_B$). Magnetization versus field data at 2 K show a steady increase in M to a maximum value of 20.6 Nβ at 5.0 T, consistent with the presence of the twenty spins expected for the two $S = 5/2$ mononuclear centers and two grids with $S = 5/2$ ground states.

Magnetic data for **3** show typical $Mn(II)_9$ grid behavior with a drop in moment per mole from 15.5 μ_B at 300 K to 6.5 μ_B at 2 K. Fitting of the data to eqs 2−4 gave $g = 1.95$, $J = -5.8$ cm^{-1}, $\alpha = 0.004$, TIP = 0 emu·mol^{-1}, and $\Theta = -3$ K ($10^2R = 3.2$). Magnetic data for **4** show a similar drop in moment per mole from 16.7 μ_B at 300 K to 6.4 μ_B at 2 K. Fitting of the susceptibility data to eqs 2−4 gave a good fit with $g = 2.01$, $J = -4.8$ cm^{-1}, $\alpha = 0.001$, TIP = 0 emu·mol^{-1}, and $\Theta = -2$ K ($10^2R = 1.8$). Despite the quite pronounced grid distortion present in **4** (vide supra), the Mn−O−Mn angles are normal, which is consistent with the observed typical J value. Magnetic data for **5**, which contains a $Mn(II)_9$ grid cation and two Curie-like mononuclear

(26) Ménage, S.; Vitols, S. E.; Bergerat, P.; Codjovi, E.; Kahn, O.; Girerd, J.-J.; Guillot, M.; Solans, X.; Calvet. *Inorg. Chem.* **1991**, *30*, 2666.

(27) Fisher, M. E. *Am. J. Phys.* **1964**, *32*, 343.

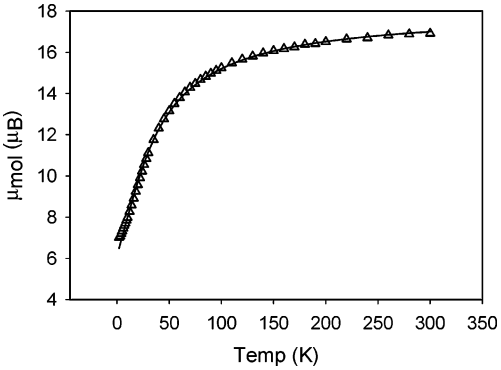

Figure 13. Magnetic properties of **1** expressed as μ_{mol} versus temperature. The solid line represents a fit to eqs 2−4 with $g = 2.028$, $J = -4.7$ cm^{-1}, $\alpha = 0.001$, TIP = 0 emu·mol^{-1}, and $\Theta = 0$ K ($10^2R = 1.9$).

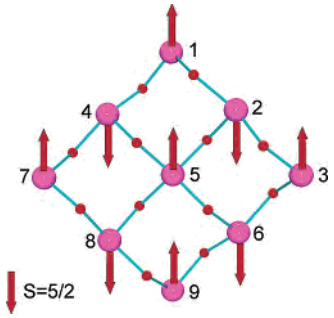

Figure 14. Spin dipole model for an antiferromagnetically coupled Mn(II)$_9$ grid system ($J \gg J'$).

Mn(II) species, show a drop in moment per mole from 19.4 μ_B at 300 K to 10.5 μ_B at 2 K. The data were fitted to eqs 2−4, adapted for the two additional mononuclear Mn(II) centers. A good data fit gave $g_{av} = 2.038$, $J = -4.1$ cm^{-1}, $\alpha = 0.0005$, TIP = 0 emu·mol^{-1}, and $\Theta = -1$ K ($10^2R = 1.5$) (see Figure S5). The good data fits for all these compounds support the chain model. The J values for **4** and **5** are typical for grids in this class and indicate that changing the terminal donor moiety (R′ = Me, Ph; Chart 1) has little effect on the exchange processes within the grid, and that the pronounced grid distortion present in **4** also has little impact on the exchange coupling situation within the grid.

Compound **6** is a mixed-oxidation-state Mn(II)/Mn(III) grid system (vide ante), on the basis of averaged metal−ligand bond lengths, and three of the corner manganese centers were found to be in the 3+ oxidation state. This would have the effect of reducing the total number of electrons in the outer ring of eight Mn centers by three, thus leading to a predictable drop in total magnetic moment. Magnetic data for **6** are shown in Figure 15 as molar susceptibility and moment versus temperature. The pronounced maximum in χ_m at 50 K for **6** is most unusual, but is of course indicative of intramolecular antiferromagnetic exchange. This differs from the Mn(II)$_9$ grids in general, where only a shoulder appears in this region, usually at lower temperatures. The plot of μ_{mol} versus temperature has the normal shape, confirming overall intragrid antiferromagnetic exchange, but the value at 2 K (2.95 μ_B) is much lower than normally observed for the Mn(II)$_9$ grids, which typically have values around 6 μ_B, and indicates a ground-state spin

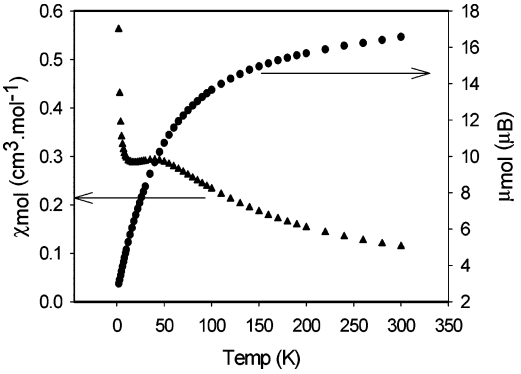

Figure 15. Magnetic properties of **6** expressed as χ_{mol} versus temperature, and μ_{mol} versus temperature.

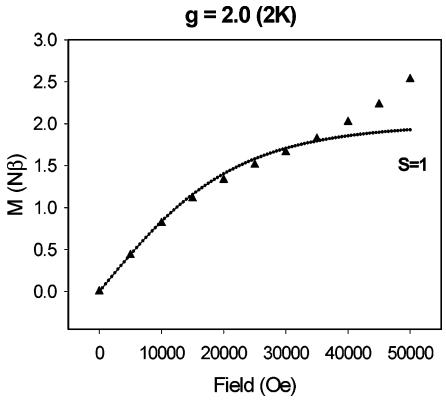

Figure 16. Magnetization data as a function of field at 2 K for **6**. The solid line was calculated using the standard Brillouin function for an $S = 1$ system up to 3.5 T.

considerably less than $S = 5/2$. In fact this value is close to what would be expected for an $S = 1$ species.

Magnetization (M) data were obtained as a function of field strength at 2 K (Figure 16), and show an increase in magnetization to a maximum of 2.5 Nβ at 5.0 T (50000 Oe), with a pronounced inflection at 3.5 T. Such behavior is typical for the Mn(II)$_9$ grids,[4] and is associated with population of upper levels in the complex spin manifold at higher fields. A good fit of the data in the lower field portion of the profile (<3.5 T) was obtained using a standard Brillouin function for an $S = 1$ system ($g = 2.0$) (solid line, Figure 16). This then defines the ground state for this complex as $S = 1$, in agreement with μ/T data. On the assumption that all other electrons are coupled antiferromagnetically, one must conclude that all the electrons in the outer ring of eight metal ions couple in an essentially isotropic manner, despite the presence of the three Mn(III) centers, and that the residual unpaired spins on the ring must interact antiferromagnetically with an equivalent number of spins on the central Mn center. This can be described by using Figure 14 with spin vectors $S = 2$ for atoms 1, 3, and 9. This is unexpected on the basis of the properties of the Mn(II)$_9$ grids as a whole, but may result from the smaller size of three of the Mn(III) centers at the grid corners, and the overall increase in Mn−O−Mn angles, which could reasonably result in J' now being significant in comparison with J. Because of the complexity of the mixed-oxidation-state exchange problem, data fitting to an exchange expres-

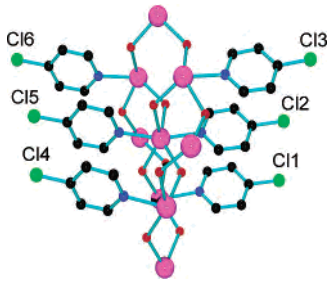

Figure 17. Core structure of **8** (POVRAY), showing the projection of the chlorine atoms (green, chlorine; black, carbon; blue, nitrogen; red, oxygen; magenta, manganese).

sion has not yet been attempted. However, both J and J' (Figure 1) would have to be considered. Magnetic data for **7** and **9**, produced by chemical oxidation of **8** with Br_2(aq), and by bulk electrochemical oxidation at 1.8 V (vide ante), respectively, are essentially identical to those of **6**, indicating that the same mixed-oxidation-state grid is produced.

Surface Studies and Implications for "Molecular Device" Behavior. The "reversibility" of the CV waves shown by **8** and **10**[1] prompted us to consider the possibility of using grid molecules arranged on a surface substrate as "bistable" or "multistable" entities capable of existing in "on" and "off" redox states, and hence storing information. The structure of **8** is typical of grids in this class, with the six chlorine atoms on the 4-positions of the central pyridine rings arranged in a roughly linear array which is projected well away from the main part of the grid itself.[6] Figure 17 shows the core structure, and the six chlorine atoms viewed roughly perpendicular to the $Mn_9(\mu\text{-}O)_{12}$ pseudoplane (Cl−Cl = 3.53−3.90 Å; Cl−Cl−Cl = 163.5° and 168.0°). The groups of three such atoms would seem ideally positioned for possible attachment of the grid molecule to a surface. Gold surfaces are relatively easy to prepare, and gold-coated substrates, e.g., gold CDs, are readily available. To test this notion, and to see if a surface-adsorbed grid molecule can be detected using electrochemical techniques, a gold foil electrode (∼3 cm^2 area) was used in place of platinum with complex **8** (CH_3CN, 1.1 × 10^{-4} M, 0.1 M TEAP, scan rate 50 mV/s) in the range 0−2 V (no electrode response in this range). Cyclic voltammetry showed two waves ($E_{1/2}$ = ∼0.9 and ∼1.3 V), in regions similar to those in which the waves observed with platinum reside, indicating a manganese-based redox response. The experiment was then repeated by first immersing a cleaned gold electrode in an acetonitrile solution of **8** for several hours, followed by thorough rinsing with acetonitrile, and then running cyclic voltammetry with just pure acetonitrile (0.1 M TEAP). A significant nonelectrode response was observed between 0.5 and 1.0 V, with a strong anodic wave at 1.62 V, clearly indicating the presence of electrode-bound grid molecules, with the most likely points of attachment being the projecting chlorine atoms.

To enhance surface binding of the grid to, e.g., gold, replacing the chlorine atoms in **8** with sulfur-based groups would be a logical step. Ligand modifications to include, e.g., S^- at the 4-pyridine position (S2poap; Chart 1, R = S^-) were effected by conversion of ammonium 2,6-dicarbethoxypyridine-4-thiolate to the corresponding hydrazide,

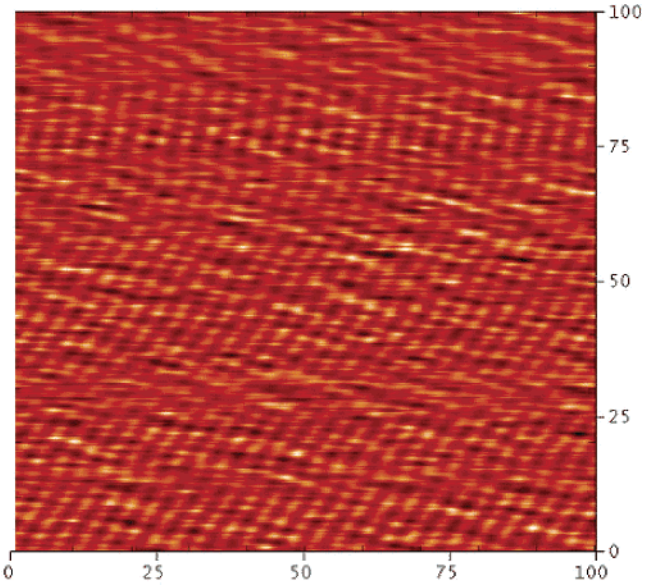

Figure 18. STM image of monolayer coverage of **12** on Au(111) (scan size 100 nm × 100 nm; tunneling conditions 50 mV, 60 pA, and ∼10^{-5} M concentration).

followed by the usual elaboration of the ligand ends by condensation with the imino ester of 2-picolinic acid.[28] Reaction of S2poap in acetonitrile with excess $Mn(ClO_4)_2 \cdot 6H_2O$ produced a red crystalline product analyzing as $[Mn_9(S2poap)_6](ClO_4)_{10} \cdot 12H_2O$ (**12**). Variable-temperature magnetic data show a typical room temperature moment of 16.8 μ_B, consistent with nine Mn(II) centers in an antiferromagnetically coupled grid, similar to, e.g., **1**, which drops to 8.3 μ_B at 2 K. The value at 2 K is somewhat higher than usual, and suggests a different internal exchange structure, perhaps due to the influence of the appended sulfur atoms, and their effect on the electronic situation within the grid. Further details on this and related complexes will be published elsewhere.[28]

Initial surface studies[18] show that when gold-coated substrates[29] are exposed to 10^{-5} to 10^{-7} M solutions of **12** in acetonitrile for 20−40 min periods, monolayer assemblies of grid molecules are formed on the gold(111) surface. Surface imagery using STM techniques, and enhanced using Fourier transform methods to effectively flatten the gold surface, is illustrated in Figure 18. Ribbons of grid molecules (bright spots) are arranged side by side, with grid dimensions on the order of 2.6 × 2.6 nm, with 3.7 nm spaces in between. Such dimensions are entirely consistent with the external size of, e.g., complex **8** (∼20 × 20 Å), estimated from crystallographic studies,[6] and indicate that the grid cations are attached to the gold surface in a flat conformation, presumably by the sulfur atoms on the ligand central pyridine rings. Figure 19 shows a space-filling model of the Mn_9 grid cation in the chloro complex **8** oriented in a projected flat surface arrangement. It represents a model for **12**, and the green spheres are intended to represent sulfur atoms. Cross-

(28) Xu, Z.; Milway, V. A.; Thompson, L. K. Unpublished results.
(29) Mazurkiewicz, J. H.; Mearns, F. J.; Losic, D.; Weeks, L.; Waclawik, E. R.; Rogers, C. T.; Shapter, J. G.; Gooding, J. J. *J. Vac. Sci. Technol.* **2002**, *B20*, 2265.

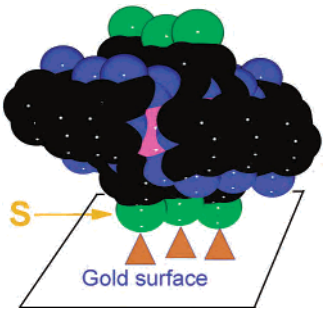

Figure 19. Surface model for **12**, based on the structure of the chloro complex **8**.

sectional imagery at low surface coverage for **12** also reveals features which are sensibly assigned to the sulfur atoms attached to the outer grid surface (Figure 19).[18]

Perchlorate anions present in **12** were not detected, and are probably beyond the resolution limit of the STM experiment. Therefore, it is not possible to estimate the charged state of the surface-bound grids. However, conduction electrons in the gold may create regions of negative charge on the surface and compensate some, or all, of the anion charge. Recent surface studies with **8** applied to Au(111)[30] show that the individual grid molecules are attached to the gold surface, with overall grid dimensions of $\sim 3 \times 3$ nm, indicating flat surface attachment, and that the chlorine atoms bound to the ligand central pyridine 4-position are also good candidates for strong surface binding, thus confirming the electrochemical results.

Conclusions and Perspectives

The use of a "bottom up" approach to nanometer-scale molecules with device capability relies heavily on molecular design, particularly of a ligand. With the appropriate coordination information encoded into the ligand itself, self-assembly has been shown to be very successful in generating novel polynuclear assemblies with ordered, and to some extent predictable, arrays of metal ions in close proximity. Ligands based on the picolinic dihydrazide central core (Chart 1) have been particularly successful in this regard, as they bring together nine metal ions, e.g., Mn(II), in close proximity, bridged by small alkoxide oxygen atoms, which ensure that electronic and magnetic communication occurs between the metal centers. Electronic "multistability" has been demonstrated, and a sulfur-derivatized grid has been applied to a gold surface. The stage is now set for further studies to address individual molecules on the surface to possibly store information. This can be envisaged in terms of an on and off condition in which the $Mn(II)_9$ grid is successively oxidized and reduced, as demonstrated with the electrochemical studies. Efforts to achieve this goal are under way. Given the close proximity of the sulfur-based grids on gold, data storage capacity can be envisaged at the level of hundreds of TB/in.^{2}, on the simple basis of one information "bit" per grid.

Acknowledgment. We thank the Natural Sciences and Engineering Research Council of Canada (NSERC) (L.K.T.), the Research Council of Norway (H.G.), the Flinders Institute of Research in Science and Technology (FIRST), and the Australian Research Council (ARC) (J.G.S., L.W.) for financial support for this work. We also thank Dr. R. McDonald, University of Alberta, for structural data.

Supporting Information Available: X-ray crystallographic data in CIF format for **1**−**6**, structural representations for **2** (Figures S1−S3) and magnetic plots for **2** (Figure S4) and **5** (Figure S5) This material is available free of charge via the Internet at http://pubs.acs.org. The CIF data have also been deposited with the Cambridge Crystallographic Data Center (CCDC), CCDC Nos. 224148−224152 and 202749. Copies of this information may be obtained free of charge from The Director, CCDC, 12 Union Rd., Cambridge CB2 1EZ, U.K. (fax +44-1223-336033; e-mail deposit@ccdc.cam.ac.uk).

IC030319V

(30) Shapter, J. G.; Weeks, L.; Thompson, L. K.; Pope, K. J.; Xu, Z,; Johnston, M. R. *Proc. SPIE*, in press.